Mechanistic Study of CO_2 Photoreduction in Ti Silicalite Molecular Sieve by FT-IR Spectroscopy

N. Ulagappan and H. Frei*

Physical Biosciences Division, Mailstop Calvin Laboratory, Lawrence Berkeley National Laboratory, University of California, Berkeley, California 94720

Received: April 18, 2000; In Final Form: June 16, 2000

The initial products of the photoreduction of gaseous CO_2 in Ti silicalite molecular sieve using methanol as electron donor have been monitored by in-situ FT-IR spectroscopy. Reaction was induced by 266 nm excitation of the $Ti^{+IV}-O^{-II} \rightarrow Ti^{+III}-O^{-I}$ ligand-to-metal charge-transfer transition of the framework center. HCO_2H, CO, and HCO_2CH_3 were the observed products. CO escaped instantaneously into the gas phase and was recorded at high spectral resolution. The origin of the products was elucidated by infrared analysis of experiments with $C^{18}O_2$, $^{13}CO_2$, and $^{13}CH_3OH$. The results show that CO originates from secondary photolysis of HCO_2H, while HCO_2CH_3 emerges mainly from spontaneous Tishchenko reaction of $CH_2{=}O$, the initial oxidation product of methanol. The key finding is that formic acid is the primary 2-electron reduction product of CO_2 at the LMCT-excited Ti centers. This implies that C−H bond formation occurs in the initial steps of CO_2 activation at the gas−micropore interface.

Introduction

Reduction of CO_2 by visible light through an endoergic reaction is one of the most attractive, yet-unrealized goals in solar energy-to-fuel conversion. Most approaches to CO_2 reduction using heterogeneous photochemistry involve the liquid−solid or gas−solid interface of semiconductor materials. Examples are TiO_2, $SrTiO_3$, or SiC in single-crystal or powder form.[1,2] The bulk of the work thus far has been conducted on aqueous suspensions of colloidal particles of TiO_2, ZnS, ZnSe, CdSe, etc., often surface-modified to enhance efficiency, selectivity, or wavelength response.[3,4] Reduction is typically initiated by transfer of photogenerated conduction band electrons to surface-adsorbed CO_2 or carbonate. Excitation wavelengths are limited to the UV region for those materials that are stable under use (metal oxides). Visible-light-induced reduction of CO_2 to CO or formic acid has been achieved with low band gap semiconductor particles such as ZnSe, ZnS, or CdS, but these materials require sacrificial reductants in order to suppress irreversible oxidation of the material. Likewise, visible light-activation of CO_2 in the presence of transition-metal colloids requires sacrificial organic donors.[5]

A second, very recent heterogeneous approach to CO_2 photoreduction employs microporous silicates containing Ti centers in the framework (TS-1, TiMCM-41 and −48).[6,7] Reactions are conducted in aqueous suspensions or on molecular sieve loaded with gaseous CO_2 and H_2O. Efficiencies of CO_2 reduction to methanol or methane in these micro- or mesoporous materials by UV light are found to be substantially enhanced compared to semiconductor TiO_2 particles. This effect, already noted in the case of dispersed Ti oxide species anchored on porous glass[8,9] or occluded in zeolite cages,[10] is attributed to the presence of isolated, tetrahedrally coordinated Ti centers. Lifetimes of the excited Ti−O charge transfer state of such framework centers were found to be several orders of magnitude longer than in the case of dense phase TiO_2 particles.[6] However, the mechanism of CO_2 photoreduction in Ti framework substituted molecular sieves remains unknown as monitoring of the reaction has thus far been conducted by gas-chromatographic analysis of the desorbed final products (CH_3OH, CH_4). Knowledge of elementary steps of this reaction at the gas−micropore interface would furnish crucial insights for the selection of new framework metals and porous structures that may afford activation of CO_2 at longer photolysis wavelengths.

In this paper, we report an in-situ FT-IR spectroscopic study of the photoreduction of CO_2 in Ti silicalite (TS-1) molecular sieve by UV light using CH_3OH as electron source. Methanol was chosen because the 2-electron-transfer reaction of CO_2 with CH_3OH involves endothermicities which, in principle, render this transformation accessible to visible photons.

Experimental Section

TS-1 molecular sieve was prepared according to the promoter-induced enhancement method reported by Kumar et al.[11,12] A gel of molar composition SiO_2:0.02 TiO_2:0.4 TPAOH:0.067 H_3PO_4:0.75 ^{i}PrOH:25 H_2O was prepared using tetraethyl orthosilicate (Aldrich, 98%), tetrabutyl orthotitanate (Fluka), and tetrapropylammonium hydroxide (TPAOH, Fluka), phosphoric acid (87%, Fluka), and 2-propanol (^{i}PrOH) as respective source materials. The gel was autoclaved at 433 K for 8−12 h. Calcination was conducted at 723 K for 10 h under flow of oxygen. ICP-AES combined with chemical analysis indicated a Ti/Si ratio of 2.6 ± 0.2%. Characterization by powder XRD (Cu Kα) was conducted in the range $5° < 2\theta < 40°$ at 0.05°/s. The resulting pattern matches exactly a simulated MFI pattern. No additional peak was found, which confirms that the material is TS-1 with no other phase present.[12,13] Also, no additional phase could be discerned from SEM pictures. The silicalite (S-1) sieve used in this study was prepared by the same procedure as TS-1 without the titanium source.

* Author to whom correspondence should be addressed.

10.1021/jp001470i CCC: $19.00
Published on Web 07/29/2000

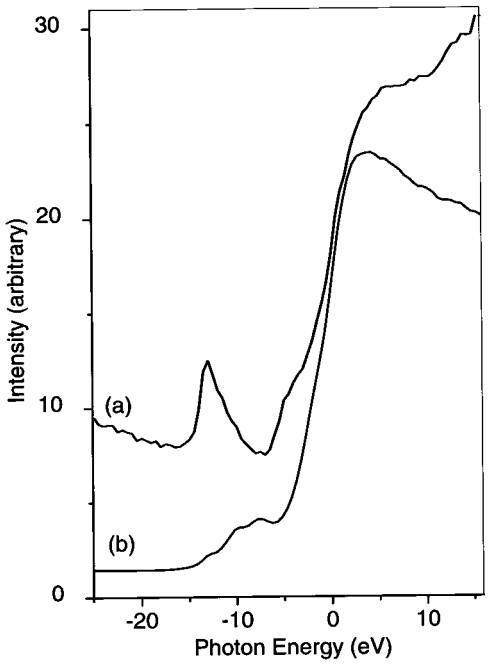

Figure 1. XANES spectra of TS-1 molecular sieve (a) and of anatase (b). Samples were prepared in the form of pressed wafers. Energy is referenced to the inflection point of the K-edge.

Ti K-edge XANES spectra were recorded at beamline 9.3.1 of the Advanced Light Source at LBNL. The beamline is equipped with a Si (111) double crystal monochromator, and ring currents were in the 200−400 mA range (1.5 GeV). Measurements were conducted in transmission mode using a Si photodiode detector, Hamamatsu model S2744-08. For energy calibration, a 5 μ Ti foil was used, and the beam intensity was monitored by the current generated at an Al foil. Self-supporting pellets of about 30 mg and 12 mm diameter were used. Samples were evacuated at 2×10^{-7} Torr, but no heating for removal of residual water was performed. Spectra were recorded in the range 4900−5100 eV at 0.5 eV sampling intervals and 3 s sampling time per data point. Figure 1 shows XANES spectra of TS-1 (trace a) and anatase (trace b). The sharp preedge peak of the TS-1 spectrum (fwhm = 2.7 eV) is characteristic of Ti in tetrahedral substitution environment of the silicalite framework (A_1-T_2 transition). Trace a agrees with the spectrum of pure TS-1 samples reported in the literature.[14,15] By contrast, the XANES spectrum of anatase shows three preedge peaks corresponding to Ti in octahedral environment.[15] No such features are observed in the TS-1 sample.

A UV−vis diffuse reflectance spectrum of calcined TS-1 in ambient air is displayed in Figure 2. It was recorded on a Shimadzu model UV-2100 spectrometer equipped with an integrating sphere model ISR-260. For this measurement, the sample was prepared in the form of a pressed wafer, and $BaSO_4$ powder used as reference. The spectrum agrees with that of TS-1 materials reported in the literature[14,17] and is assigned to the $Ti^{+IV}-O^{-II} \rightarrow Ti^{+III}-O^{-I}$ ligand-to-metal charge-transfer transition of tetrahedrally coordinated Ti (perfect or distorted).[18,19] There is no indication of extraframework Ti-containing species, which are known to give rise to absorption at wavelengths longer than 330 nm.[14,17] Specifically, we do not observe any shoulder at 370 nm, indicative of anatase impurity. Spectra of neat anatase and of anatase (2%) mixed with TS-1 are shown in Figure 2 for comparison. On the basis of comparison of our XANES and UV−vis spectra with data reported in the literature,[14,17] we conclude that the TS-1 sample contains no extraframework species.

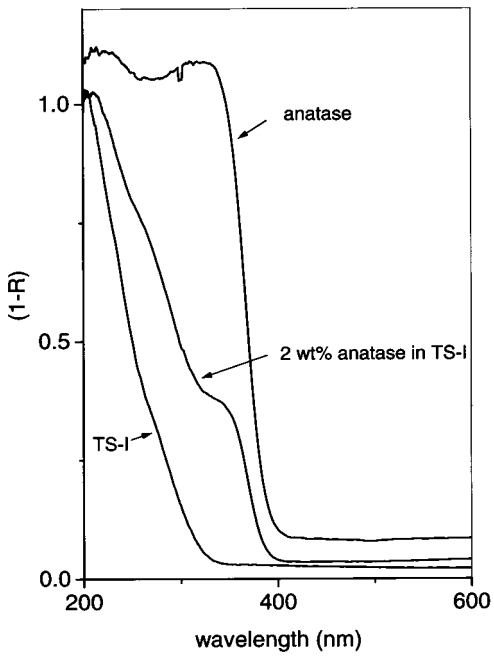

Figure 2. Diffuse reflectance spectra of pressed wafers of TS-1 molecular sieve, neat anatase, and a mixture of anatase (2%) and TS-1 crystallites.

Photochemical experiments were conducted using equipment and procedures described previously.[20] In brief, about 22 mg of TS-1 powder was pressed into a self-supporting wafer (3 min under a pressure of 2×10^5 kPa). The TS-1 wafer was held in a miniature infrared vacuum cell, equipped with CaF_2 windows, which was mounted inside an Oxford cryostat model Optistat. Dehydration of the sieve was accomplished by heating to 473 K under high vacuum (temperature controller Oxford model ITC-502). Reactants were loaded into the molecular sieve from the gas phase through a vacuum manifold. Chemistry was monitored in situ by infrared spectroscopy, using an IBM-Bruker spectrometer model IR-97 at 1 cm^{-1} and 0.1 cm^{-1} resolution. Photolysis was typically conducted at room temperature using the 266 nm emission of a pulsed Nd:YAG laser at 10 Hz (model Quanta-Ray DCR-2A with GCR3 upgrade).

Methanol (EM Science, 99%), $^{13}CH_3OH$ (Aldrich, 95% ^{13}C), CD_3OD (Aldrich, 99.5% D), formic acid (Aldrich, 95%), and $H^{13}CO_2H$ (Aldrich, 99% ^{13}C) were degassed by vacuum distillation. Paraformaldehyde (Aldrich, 95%) was depolymerized and purified as described in the literature.[21] CO_2 (Matheson, 99.995%), $^{13}CO_2$ (ISOTEC, Inc., 99.1% ^{13}C, 99.97% ^{16}O), $C^{18}O_2$ (Prochem, 99.4% ^{18}O), CO (Matheson, 99.99%), ^{13}CO (ISOTEC, Inc., 99% ^{13}C), and $C^{18}O$ (ISOTEC, Inc., 95% ^{18}O) were used as received.

Results

1. Infrared Spectrum of CO_2 Adsorbed on TS-1 Sieve. Loading of CO_2 gas into the IR cell containing TS-1 sieve gave rise to infrared absorptions at 1381, 1663, 2276 (natural abundance of $^{13}CO_2$), 2346, 3597, 3629, and 3704 cm^{-1}. For $C^{18}O_2$, corresponding bands were at 1334, 1633, 2310, 3515, 3534, 3625, and 3656 cm^{-1}, and for $^{13}CO_2$ at 1366, 1619, 2280, 3511, 3541, 3625, and 3646 cm^{-1}. Comparison with literature spectra[22] shows that the intense asymmetric stretch at 2346 cm^{-1} ($^{12}C^{16}O_2$) and the combination tones in the 3500−3700 cm^{-1} region originate from both gas-phase and adsorbed CO_2 (the volume of the infrared vacuum cell is 3.4 cm^3, with a path length of 3 cm). The same observation was made for the corresponding

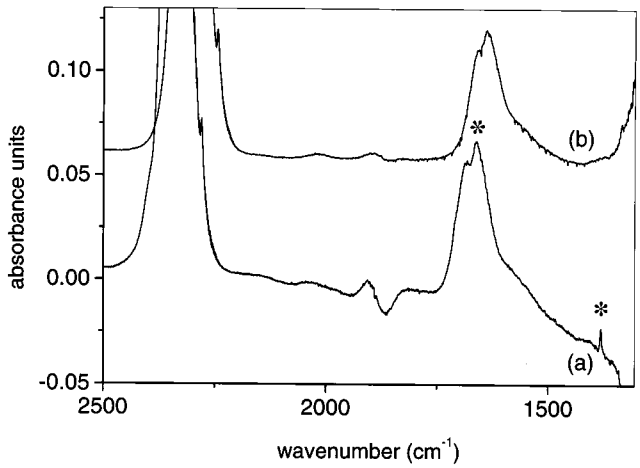

Figure 3. Infrared difference spectra upon loading of 20 Torr of CO_2 (a) or $C^{18}O_2$ (b) into TS-1 sieve at room temperature. Bands marked by asterisk are unique to adsorbed CO_2.

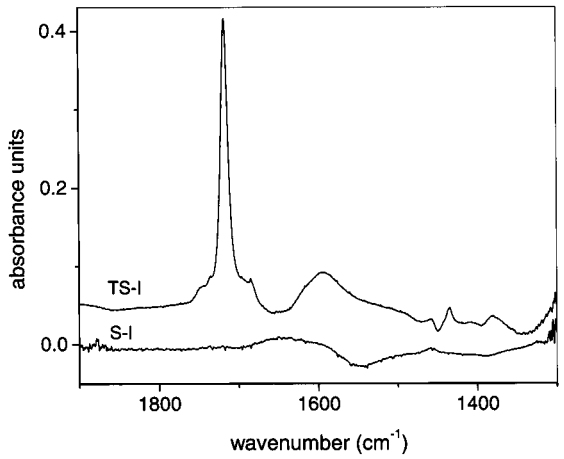

Figure 4. Infrared difference spectra upon 4 h irradiation at 266 nm (30 mW cm^{-2}) of a mixture of CH_3OH (5 Torr) and CO_2 (40 Torr) adsorbed into TS-1 or silicalite (S-1) sieve.

bands of $^{13}CO_2$ and $C^{18}O_2$. By contrast, the broad absorption around 1670 cm^{-1} (main peaks at 1663 cm^{-1} ($^{12}C^{16}O_2$), 1633 cm^{-1} ($C^{18}O_2$) and 1619 cm^{-1} ($^{13}CO_2$)) and the sharp feature at 1381 cm^{-1} (1334 cm^{-1} ($C^{18}O_2$) and 1366 cm^{-1} ($^{13}CO_2$)) are only observed for CO_2 adsorbed on TS-1. Corresponding spectra for CO_2 and $C^{18}O_2$ are shown in Figure 3. The 1381 cm^{-1} band is assigned to the ν_1 symmetric stretch as the frequency and isotope shifts agree with reported Raman spectra.[22] Since this is an infrared forbidden mode for the unperturbed molecule, it is induced by interaction with the micropore environment. Framework Ti centers seem principally responsible for activation of this band because its intensity is greatly diminished in neat silicalite sieve. The 1663 cm^{-1} absorption exhibits an ^{18}O shift of 30 cm^{-1} and a ^{13}C shift of 44 cm^{-1}, typical for ν(C═O) of a O═C−O moiety.[23] The absorption can readily be removed by evacuation of the sieve, which suggests that it originates from weakly adsorbed CO_2 molecules. Since loading of the gas into silicalite sieve also results in an absorption around 1670 cm^{-1}, the band is attributed to interaction of CO_2 with silicous regions of the micropores.

2. Photoreaction of CO_2 and CH_3OH in TS-1. Loading of 5 Torr of methanol gas into dehydrated TS-1 sieve at room temperature resulted in infrared absorptions at 1350, 1450, 1463, 2847, 2952, 2988, 3280, and 3623 cm^{-1}. The bands at 3250 and 3623 cm^{-1} signal the presence of CH_3OH molecules with free OH groups (3623 cm^{-1}) as well as molecules H-bonded to the pore wall (3250 cm^{-1}, very broad). Coadsorption of 40 Torr CO_2 into the sieve did not result in any reaction. When irradiating the loaded matrix with 266 nm light, depletion of CO_2 and methanol was observed under concurrent growth at 1380, 1434, 1461, 1594, 1717, 2856, and 2963 cm^{-1}. An FT-IR difference spectrum following the 4 h irradiation at 266 nm (30 mWcm^{-2}) is shown in Figure 4. When conducting the same irradiation experiment on a neat silicalite matrix (S-1) loaded with CO_2 and CH_3OH, no product growth was observed (Figure 4). Clearly, photochemical reaction requires the presence of Ti centers. The bands at 1717 and 1434 cm^{-1} agree with those of an authentic sample of HCO_2CH_3 in TS-1, as do the ν(C−H) absorptions at 2856 and 2963 cm^{-1}. Methyl formate has an additional peak at 1456 cm^{-1}, which overlaps in the CO_2 + CH_3OH photolysis spectrum with the decreasing methanol absorption at 1450 cm^{-1} and, hence, is shifted to 1461 cm^{-1}. These methyl formate bands agree well with the infrared spectrum of matrix isolated HCO_2CH_3 reported in the literature.[24] Spectra of HCO_2H gas loaded into TS-1 indicate that

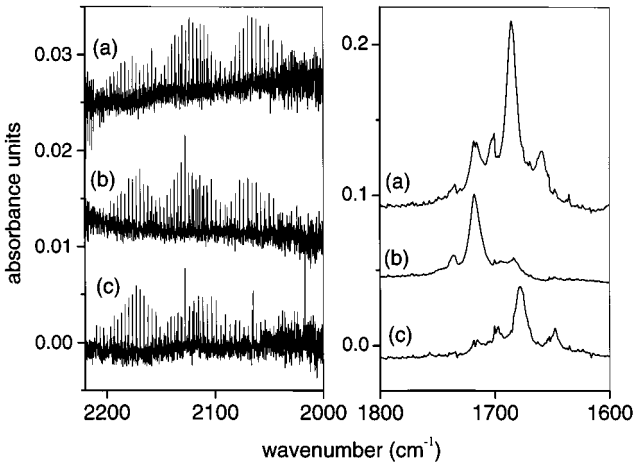

Figure 5. Infrared difference spectra following 4 h photolysis of $C^{18}O_2$ + CH_3OH (a), $^{13}CO_2$ + CH_3OH (b), and CO_2 + $^{13}CH_3OH$ (trace c) loaded into TS-1 sieve. Spectra in the 2200−2000 cm^{-1} region were recorded at 0.1 cm^{-1} resolution; those in the fingerprint region at 1 cm^{-1} resolution.

the product peak at 1380 cm^{-1} originates from formic acid. The C═O stretch of HCO_2H overlaps with the HCO_2CH_3 absorption at 1717 cm^{-1}. HCO_2H loaded into TS-1 exhibits, in addition, a broad band at 1594 cm^{-1} that coincides with a similarly shaped band in the CO_2 + CH_3OH photoreaction spectrum. Since this feature is only present in silicalite sieves containing framework Ti, and is at a frequency typical for the asymmetric CO_2 stretch of formate,[25] it is attributed to $\nu_{as}(CO_2)$ of formate interacting with Ti centers, HCO_2- - -Ti. This assignment is confirmed by the expected ^{13}C, ^{18}O, and D frequency shifts. The only other product absorptions of CO_2 + CH_3OH photolysis in TS-1 were those due to gas-phase CO in the 2100−2200 cm^{-1} region. Recording of these bands required a spectral resolution of 0.1 cm^{-1}. The fact that carbon monoxide produced in TS-1 desorbs quantitatively from the sieve is not surprising given the weak adsorption tendency of CO in room-temperature silicalite.

To determine the origin of these products, photolysis experiments were conducted with $C^{18}O_2$, $^{13}CO_2$, and $^{13}CH_3OH$. Figure 5 shows the infrared difference spectra following 266 nm irradiation of TS-1 sieve loaded with $C^{18}O_2$ + CH_3OH (trace a), $^{13}CO_2$ + CH_3OH (trace b), and CO_2 + $^{3}CH_3OH$ (trace c). Spectra shown in the 1800−1600 cm^{-1} region were recorded at 1 cm^{-1} resolution; those in the 2200−2000 cm^{-1} region were taken at 0.1 cm^{-1} resolution. Comparison of product bands in

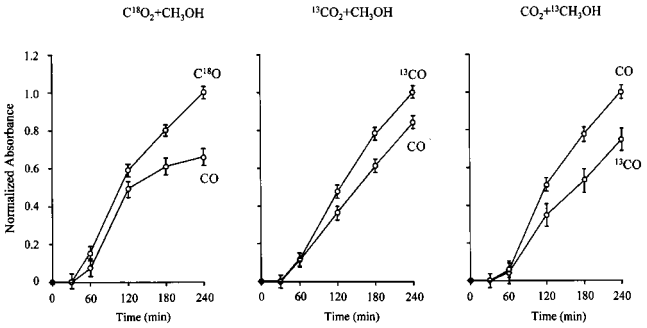

Figure 6. Kinetics of infrared absorbance growth of carbon monoxide upon photolysis of $C^{18}O_2 + CH_3OH$, $^{13}CO_2 + CH_3OH$, and $CO_2 + {}^{13}CH_3OH$ in TS-1 sieve. Curves represent the average of the normalized peak absorbance growth of all ro-vibrational bands of a given isotopic species, shown in Figure 5. For each reaction, the curves of the two isotopic CO products reflect the relative amounts produced.

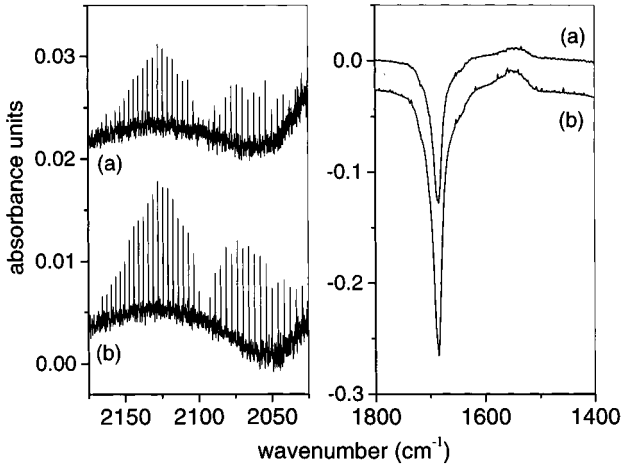

Figure 7. Photolysis of $H^{13}CO_2H$ loaded into TS-1 sieve at 266 nm (30 mW cm^{-2}). (a) Infrared difference spectrum following 15 min irradiation, (b) 30 min irradiation. Spectra in the 2200−2000 cm^{-1} region were recorded at 0.1 cm^{-1} resolution, those below 2000 cm^{-1} at 1 cm^{-1} resolution.

the 2200−2000 cm^{-1} region with gas-phase spectra of authentic samples of CO, $C^{18}O$, and ^{13}CO affords complete assignment of all ro-vibrational peaks.[26] According to Figure 5, $C^{18}O$ is the main carbon monoxide species formed upon $C^{18}O_2 + CH_3OH$ photolysis, while ^{13}CO dominates in the $^{13}CO_2 + CH_3OH$ reaction, and parent CO is the main species produced upon $CO_2 + {}^{13}CH_3OH$ photolysis. The growth kinetics of the CO product displayed in Figure 6 for each of the three isotopic experiments clearly exhibits an induction period indicative of secondary photolysis. Irradiation of TS-1 matrices loaded with authentic samples of formic acid indicate that carbon monoxide is generated by efficient photolysis of the acid. This is illustrated in Figure 7 by infrared difference spectra recorded upon 266 nm irradiation of $H^{13}CO_2H$ in TS-1 for 15 min (trace a) and 30 min (trace b) at 30 mW cm^{-2}. We conclude that the carbon monoxide product of the carbon dioxide + methanol photoreaction originates from secondary photolysis of formic acid. By contrast, only traces of methyl formate photodissociation were detected under the same irradiation conditions.

In the C═O stretching region, the simple product spectrum of the parent reaction $CO_2 + CH_3OH$ (Figure 4) is replaced by a complex pattern of bands when using $C^{18}O_2$, $^{13}CO_2$, or $^{13}CH_3OH$ as reactants (Figure 5). Analysis of these spectra reveals the origin of the products. Most useful is a comparison of spectra at early photolysis times with those recorded upon prolonged irradiation. Figure 8 shows infrared difference spectra

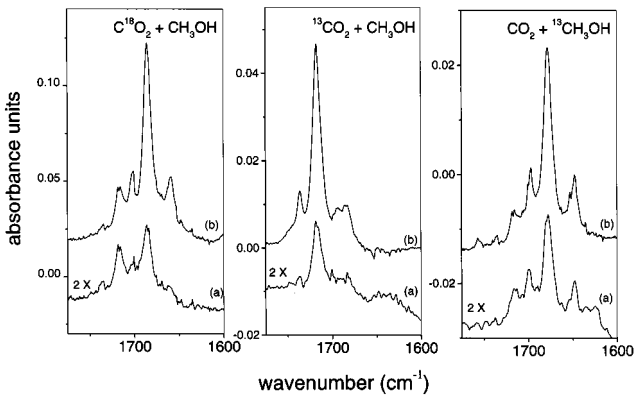

Figure 8. Absorbance growth behavior of $C^{18}O_2 + CH_3OH$, $^{13}CO_2 + CH_3OH$, and $CO_2 + {}^{13}CH_3OH$ upon 266 nm photolysis. (a) Infrared difference spectra after 1 h irradiation. Intensities are amplified by a factor of 2 for clarity. (b) Difference between 4 and 1 h photolysis.

upon 1 h photolysis (trace a) and of the time window between 1 and 4 h irradiation (trace b) for all three isotopic systems. Clearly, relative intensities of spectra (a) differ significantly from those of spectra (b). In the case of the $^{13}CO_2 + CH_3OH$ reaction, absorbance growth at 1682 cm^{-1} lags behind that of bands at 1736, 1717, and 1695 cm^{-1} at late photolysis times (trace b) compared to start of photolysis (trace a). The 1682 cm^{-1} peak is due to $H^{13}CO_2H$ according to the $H^{13}CO_2H$ spectrum in TS-1 (Figure 7) and literature data.[27] The 1736, 1717, and 1695 cm^{-1} bands are attributed to different sites of HCO_2CH_3 (ν(C═O)) based on authentic spectra of this molecule in TS-1. The leveling off of $H^{13}CO_2H$ growth is consistent with secondary photolysis of the acid, signaled by the appearance of ^{13}CO (Figure 5). The formation of $H^{13}CO_2H$ implies that carbon dioxide is photoreduced to formic acid. Close inspection of the band intensities at 1736, 1717, and 1695 cm^{-1} reveals that the 1717 cm^{-1} peak grows faster than the other two upon prolonged photolysis. Since HCO_2H also absorbs at 1717 cm^{-1}, this suggests increased HCO_2H growth at late photolysis times. Formation of HCO_2H is confirmed by the appearance of CO, its secondary photolysis product (Figure 5).

These assignments are fully supported by the analysis of the $CO_2 + {}^{13}CH_3OH$ system, the isotopic counterpart to the reactions just presented. Here the absorbance growth at 1717 cm^{-1} falls behind that of bands at 1696, 1679, and 1647 cm^{-1} at late photolysis times, as can clearly be seen in Figure 8. The 1717 cm^{-1} absorption is assigned to HCO_2H, and the early leveling off of its growth is consistent with the appearance of the parent isotope CO as the dominant carbon monoxide product of the reaction (Figure 5). This confirms that CO_2 is photoreduced to HCO_2H. The 1696, 1679, and 1647 cm^{-1} triplet is attributed to $H^{13}CO_213CH_3$. Analogous to the $^{13}CO_2 + CH_3OH$ case, the 1679 cm^{-1} band outpaces the growth at 1696 and 1647 cm^{-1} at long photolysis times. This indicates formation of $H^{13}CO_2H$ upon prolonged reaction, and is confirmed by the concurrent production of ^{13}CO (Figure 5). We conclude from the isotope experiments with $^{13}CO_2$ and $^{13}CH_3OH$ that carbon dioxide is directly reduced to formic acid while the carbon of the methanol appears in methyl formate and, upon prolonged photolysis, also in formic acid.

Observation of methyl formate and formic acid as methanol oxidation products, rather than the expected 2-electron oxidation product formaldehyde, can be understood by the results of CH_2═O loading into TS-1, shown in Figure 9. Spectra recorded immediately after loading of formaldehyde into the sieve exhibit the characteristic CH_2═O peaks at 1503 and 1730 cm^{-1}. The 2813, 2909, and 2975 cm^{-1} absorptions in the C−H stretching

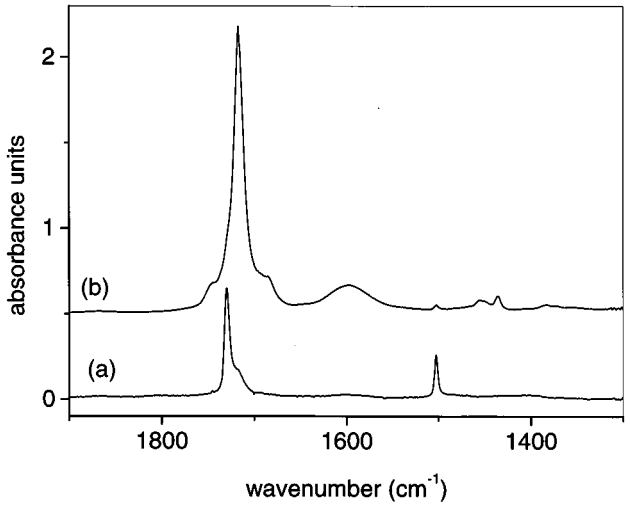

Figure 9. Spontaneous dark reaction of formaldehyde loaded into TS-1 sieve. (a) Infrared spectrum recorded immediately after loading of 5 Torr of CH_2═O. (b) Spectrum after 1 h in the dark at room temperature.

region are also observed (not shown).[28,29] After 1 h in the dark (trace b), the CH_2═O spectrum has practically disappeared and is replaced by absorptions of HCO_2CH_3 (1717, 1456, 1436 cm^{-1}). A weak band at 1383 cm^{-1} indicates the formation of small amounts of HCO_2H (which also absorbs at 1717 cm^{-1}), and of HCO_2- - -Ti absorbing at 1596 cm^{-1}. We attribute the principal product, HCO_2CH_3, to the well-known Tishchenko reaction,[30] CH_2═O + CH_2═O → HCO_2CH_3. Small amounts of HCO_2H (HCO_2- - - Ti) indicate that Cannizzaro reaction CH_2═O + CH_2═O + H_2O→ HCO_2H + CH_3OH involving residual H_2O still present after dehydration of the sieve also plays a role. The latter was the dominant process upon loading of formaldehyde into $FeAlPO_4$-5 sieve.[20] We conclude from CH_2═O spectroscopy in TS-1 that the observed methyl formate and a small fraction of the formic acid produced upon CO_2 + CH_3OH photoreaction are secondary thermal products of initially generated formaldehyde.

Analysis of the $C^{18}O_2$ + CH_3OH spectra and comparison with the ^{13}C results furnishes a detailed insight into the role of Tishchenko and Cannizzaro reactions of CH_2═O, the proposed initial oxidation product of methanol. According to Figure 5, $C^{18}O$ is the dominant carbon monoxide product of $C^{18}O_2$ + CH_3OH photolysis. Its growth exhibits an induction period, which confirms that $C^{18}O_2$ is reduced to $HC^{18}O_2H$ in the initial step. The latter absorbs at 1682 cm^{-1} and is most probably the main contributor to the band at that frequency in the early photolysis spectrum (trace a of Figure 8). In addition, spectrum (a) of the $C^{18}O_2$ + CH_3OH reaction features peaks at 1736 and 1717 cm^{-1}, which are assigned to HCO_2CH_3, most probably formed by Tishchenko reaction of CH_2═O, the primary oxidation product of CH_3OH. Interestingly, additional peaks appear in the region below 1700 cm^{-1} upon prolonged photolysis (trace b of Figure 8), indicating incorporation of ^{18}O into the secondary thermal products of CH_2═O. This can readily be explained by the formation of $H_2{}^{18}O$ upon secondary photolysis of $HC^{18}O_2H$. It opens up the Cannizzaro reaction with the continuously generated CH_2═O to form $HC^{18}OOH$ and CH_3OH. $HC^{18}OOH$ and methanol form $HC^{18}OOCH_3$ by subsequent ester condensation. $HC^{18}OOCH_3$ isotopomers with a C═^{18}O group give rise to bands at 1700, 1685, and 1659 cm^{-1}.[18] HC(═^{18}O)OH absorbs at 1685 cm^{-1} as well.[27] We conclude from the analysis of the isotopic data that formaldehyde is the initial oxidation product of methanol. In the early stages of photolysis, the aldehyde is converted to methyl formate by the Tishchenko mechanism.

SCHEME 1

Primary Photochemistry

$$CO_2 + CH_3OH \xrightarrow{h\nu} HCO_2H + CH_2{=}O$$

Secondary Reactions

$$HCO_2H \xrightarrow{h\nu} CO + H_2O$$

$$2\,CH_2{=}O \xrightarrow{\text{dark}} HCO_2CH_3 \quad \text{(initial phase)}$$

$$2\,CH_2{=}O + H_2O \xrightarrow{\text{dark}} HCO_2H + CH_3OH \quad \text{(upon accumulation of } H_2O\text{)}$$

SCHEME 2

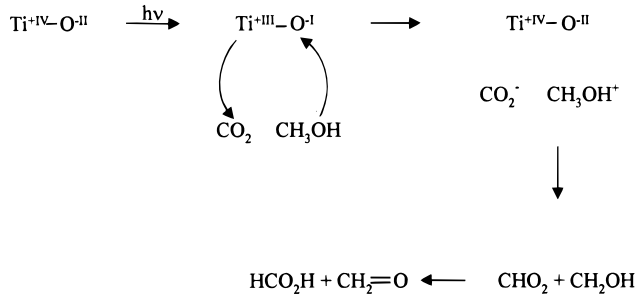

Upon continued photolysis, formaldehyde is consumed by the Cannizzaro reaction opened up by the formation of H_2O through secondary photolysis of formic acid. Scheme 1 summarizes the photochemistry derived from the spectral and kinetic analysis.

Discussion

The main result of this study is the detection of formic acid as the primary 2-electron-transfer product of CO_2 photoreduction at the gas−micropore interface of Ti silicate sieve. While the elucidation of the secondary photochemical and dark processes proved essential for establishing the nature of the initial 2-electron redox process, it is the latter that is of foremost interest; secondary reactions, in particular the photodissociation of formic acid, may not occur once materials are found that allow initiation of the photochemistry at substantially longer wavelengths.

Our proposed mechanism for Ti−O LMCT-induced reaction of CO_2 and CH_3OH consists of two one-electron-transfer steps. Upon excitation of the metal center, transient Ti^{+III} reduces CO_2 to CO_2^- under concurrent oxidation of methanol to the radical cation by the hole on the oxygen ligand, as shown in Scheme 2. Proton transfer quenching of the highly unstable CO_2^- by the strongly acidic CH_3OH^+ [31] would result in CHO_2 radical and CH_3O radical. The latter most probably isomerizes to the more stable CH_2OH radical.[29,32] Subsequent H atom transfer to yield HCO_2H and CH_2═O affords overall 2-electron reduction of CO_2.

The energy profile of the proposed mechanism depends to a substantial degree on the structure of the proposed CHO_2 intermediate. Gas-phase CHO_2 radical is known to exist in two isomeric forms, namely, HCO_2 (formate)[33] and HOCO (hydroxy

carbonyl).[34,35] On the basis of enthalpies of formation ($\Delta H_f°(CO_2) = -94.05$ kcal mol^{-1} [36]; $\Delta H_f°(CH_3OH) = -48.0$ kcal mol^{-1} [36]; $\Delta H_f°(CH_2OH) = -2$ kcal mol^{-1} [37]; $\Delta H_f°(HCO_2) = -31$ kcal mol^{-1} [33]; $\Delta H_f°(HOCO) = -51$ kcal mol^{-1} [33]), we estimate an endothermicity of 109 kcal mol^{-1} for the $CO_2 + CH_3OH \rightarrow HCO_2 + CH_2OH$ path, and 87 kcal mol^{-1} for the $HOCO + CH_2OH$ route. Hence, the formation of HOCO intermediate is thermodynamically preferred, and is consistent with the fact that the reaction can be initiated by 266 nm quanta (107 kcal mol^{-1}). By contrast, the photolysis photon energy is a few kcal mol^{-1} short of generating formate radical. However, the thermochemical data refer to the free species in the gas phase. Interaction of the transient radicals with the Ti center may lower these energies substantially. While we cannot be more specific on the CHO_2 intermediate, this work establishes conclusively that single photon-induced 2-electron reduction of CO_2 at Ti centers in the silicate framework results in the formation of a C−H bond, and not in abstraction of oxygen to yield CO.

Anpo and co-workers have proposed a mechanism for CO_2 photoreduction by H_2O in Ti silicate sieves,[6,7] based on spectroscopic studies using highly dispersed Ti oxide anchored on porous glass, or by using powdered TiO_2 catalyst.[38,39] ESR measurements at 77 K of CO_2 photoreduction at these surfaces indicate the formation of Ti^{3+} ions, H atoms and OH radicals, and C radicals. When conducting the photoreaction at 323 K, CH_3OH, CH_4, and CO were detected as products. From these results, it was proposed that CO_2 reduction and H_2O decomposition proceed competitively at the LMCT- excited Ti−O centers; CO_2 is reduced to CO, and subsequently to C radicals while H_2O photodecomposes to H and OH radicals. Reaction of H and OH with the carbon species is thought to yield CH_3OH and CH_4.[6,38,39] It is not known how many photons are consumed by these transformations. While the mechanism proposed by Anpo cannot be compared directly with the CO_2 photoreduction reported here because of the use of different electron donors, it is important to note that, according to our results, formic acid photodissociates efficiently to CO and H_2O under UV irradiation of the Ti−O LMCT transition. Hence, formation of HCO_2H might escape detection under continuous UV photolysis conditions.

Conclusions

In-situ FT-IR monitoring of the Ti−O LMCT-induced photoreduction of gaseous CO_2 in Ti silicalite sieve using methanol as donor has revealed formic acid as the primary 2-electron-transfer product. This establishes C−H bond formation during the initial steps of CO_2 photoreduction. While carbon monoxide product is also observed, the growth kinetics indicate that CO is formed by secondary photolysis of HCO_2H. This study constitutes the first insight into the initial steps of CO_2 photoreduction in a framework Ti molecular sieve. The proposed mechanism involves photoinduced one-electron transfer to produce transient CHO_2 radical. Time-resolved infrared spectroscopic studies on the nanosecond time-scale will be needed to detect this crucial intermediate and elucidate its structure.[40−42]

Acknowledgment. This work was supported by the Director, Office of Science, Office of Basic Energy Sciences, Chemical Sciences Division of the U.S. Department of Energy under Contract No. DE-AC03-76SF00098.

References and Notes

(1) Hemminger, J. C.; Carr, R.; Somorjai, G. A. *Chem. Phys. Lett.* **1978**, *57*, 100.
(2) Inoue, T.; Fujishima, A.; Konishi, S.; Honda, K. *Nature* **1979**, *277*, 637.
(3) Halmann, M. M. *Chemical Fixation of Carbon Dioxide*; CRC Press: Boca Raton, 1993; p 131.
(4) Linsebigler, A. L.; Lu, G.; Yates, J. T., Jr. *Chem. Rev.* **1995**, *95*, 735.
(5) Mandler, D.; Willner, I. *J. Am. Chem. Soc.* **1987**, *109*, 7884.
(6) Anpo, M.; Yamashita, H.; Ikene, K.; Fujii, Y.; Zhang, S. G.; Ichihashi, Y.; Park, D. R.; Susuki, Y.; Koyano, K.; Tatsumi, T. *Catal. Today* **1998**, *44*, 327, and references therein.
(7) Zhang, S. G.; Fujii, Y.; Yamashita, H.; Koyano, K.; Tatsumi, T.; Anpo, M. *Chem. Lett.* **1997**, 659.
(8) Chiba, K.; Anpo, M. *J. Mol. Catal.* **1992**, *74*, 207.
(9) Anpo, M.; Yamashita, H. In *Surface Photochemistry*; Anpo, M., Ed.; Wiley: Chichester, 1996; p 117.
(10) Anpo, M.; Yamashita, H.; Ichihashi, Y.; Fujii, Y.; Honda, M. *J. Phys. Chem. B* **1997**, *101*, 2632.
(11) Kumar, R.; Bhaumik, A.; Ahedi, R. K.; Ganapathy, S. *Nature* **1996**, *381*, 298.
(12) Bhaumik, A.; Mukherjee, P.; Kumar, R. *J. Catal.* **1998**, *178*, 101.
(13) Treacy, M. M. J.; Higgins, J. B.; van Ballmoos, R. *Zeolites* **1996**, *16*, 524.
(14) Trong On, D.; Kaliaguine, S.; Bonneviot, L. *J. Catal.* **1995**, *157*, 235.
(15) Vayssilov, G. N. *Catal. Rev.* **1997**, *39*, 209, and references therein.
(16) Geobaldo, F.; Bordiga, S.; Zecchina, A.; Giamello, E.; Leofanti, G.; Petrini, G. *Catal. Lett.* **1992**, *16*, 109.
(17) Van der Pol, A. J. H. P.; Verduyn, A. J.; van Hoof, J. H. C. *Appl. Catal. A* **1992**, *92*, 113.
(18) Duprey, E.; Beaunier, P.; Springuel, M. A.; Bozon, F.; Fraissard, J.; Manoli, J. M.; Bregeault, J. M. *J. Catal.* **1997**, *165*, 22.
(19) Lamberti, C.; Bordiga, S.; Arduino, D.; Zecchina, A.; Geobaldo, F.; Spano, G.; Genoni, F.; Petrini, G.; Carati, A.; Villain, F.; Vlaic, G. *J. Phys. Chem. B* **1998**, *102*, 6382.
(20) Ulagappan, N.; Frei, H. *J. Phys. Chem. A* **2000**, *104*, 490.
(21) Spence, R.; Wild, W. *J. Chem. Soc. (London)* **1935**, 338.
(22) Herzberg, G. *Infrared and Raman Spectra*; Van Nostrand: New York, 1945; p 274.
(23) Jacox, M. E.; Milligan, D. E. *J. Mol. Spectrosc.* **1974**, *52*, 363.
(24) Müller, R. P.; Hollenstein, H.; Huber, J. R. *J. Mol. Spectrosc.* **1983**, *100*, 95.
(25) Colthup, N. B.; Daly, L. H.; Wiberley, S. E. *Introduction to Infrared and Raman Spectroscopy*, 3rd ed.; Academic Press: New York, 1990; p 317.
(26) Plyler, E. K.; Danti, A.; Blaine, L. R.; Tidwell, E. D. *J. Res. Natl. Bur. Stand.* **1960**, *64*, 29.
(27) Redington, R. L. *J. Mol. Spectrosc.* **1977**, *65*, 171.
(28) Herzberg, G. *Infrared and Raman Spectra*; Van Nostrand: New York, 1945; p 300.
(29) Jacox, M. E. *Chem. Phys.* **1981**, *59*, 213.
(30) March, J. *Advanced Organic Chemistry*, 4th ed.; Wiley: New York, 1992; p 1233.
(31) Hammerich, O.; Parker, V. D. *Adv. Phys. Org. Chem.* **1984**, *20*, 55.
(32) (a) Radford, H. E. *Chem. Phys. Lett.* **1980**, *71*, 195. (b) Radford, H. E.; Evenson, K. M.; Jennings, D. A. *Chem. Phys. Lett.* **1981**, *78*, 589.
(33) Kim, E. H.; Bradforth, S. E.; Arnold, D. W.; Metz, R. B.; Newmark, D. M. *J. Chem. Phys.* **1995**, *103*, 7801.
(34) Jacox, M. E. *J. Chem. Phys.* **1988**, *88*, 4598.
(35) Milligan, D. E.; Jacox, M. E. *J. Chem. Phys.* **1971**, *54*, 927.
(36) Benson, S. W. *Thermochemical Kinetics*; Wiley: New York, 1968.
(37) Tsang, W. In *Energetics of Organic Free Radicals*; Martinho-Simoes, J. A., Greenberg, A., Liebman, J. F., Eds.; Blackie Academic and Professional: London, 1996; p 22.
(38) Anpo, M.; Chiba, K. *J. Mol. Catal.* **1992**, *74*, 207.
(39) Anpo, M.; Yamashita, H.; Ichihashi, Y.; Ehara, S. *J. Electroanal. Chem.* **1995**, *396*, 21.
(40) Vasenkov, S.; Frei, H. *J. Am. Chem. Soc.* **1998**, *120*, 4031.
(41) Vasenkov, S.; Frei, H. *J. Phys. Chem. A* **2000**, *104*, 4327.
(42) Vasenkov, S.; Frei, H. In *Molecular and Supramolecular Photochemistry*; Ramamurthy, V., Schanze, K. S., Eds.; Marcel Dekker: New York, 2000; Vol. 5, p 299.